PCCP

Accepted Manuscript

ROYAL SOCIETY OF CHEMISTRY

www.rsc.org/pccp

Cite this: DOI: 10.1039/c0xx00000x

www.rsc.org/xxxxxx

ARTICLE TYPE

18-electron rule inspired Zintl-like ions composed of all transition metals

Jian Zhou,[a] Santanab Giri [a] and Purusottam Jena [*,a]

Received (in XXX, XXX) Xth XXXXXXXXX 20XX, Accepted Xth XXXXXXXXX 20XX

DOI: 10.1039/b000000x

Zintl phase constitutes a unique class of compounds composed of metal cations and covalently bonded multiply charged cluster anions. Potential applications of these materials in solution chemistry and thermoelectric materials have given rise to renewed interest in the search of new Zintl ions. Up to now these ions are mostly composed of group 13, 14, and 15 post-transition metal elements and no Zintl ions composed of *all* transition metal elements are known. Using gradient corrected density functional theory we show that the 18-electron rule can be applied to design a new class of Zintl-like ions composed of *all* transition metal atoms. We demonstrate this possibility by using $Ti@Au_{12}^{2-}$ and $Ni@Au_6^{2-}$ di-anions as examples of Zintl-like ions. Predictive capability of our approach is demonstrated by showing that FeH_6^{4-} in already synthesized complex metal hydride, Mg_2FeH_6, is a Zintl-like ion, satisfying the 18-electron rule. We also show that novel Zintl phase compounds can be formed by using *all* transition metal Zintl-like ions as building blocks. For example, a two-dimensional periodic structure of $Na_2[Ti@Au_{12}]$ is semiconducting and nonmagnetic while a one-dimensional periodic structure of $Mg[Ti@Au_{12}]$ is metallic and ferromagnetic. Our results open door to the design and synthesis of a new class of Zintl-like ions and compounds with potential for applications.

Introduction

Zintl ions are *multiply* negatively charged polyatomic clusters belonging to post transition metal elements in group 13, 14, and 15 (e.g. Sn_5^{2-}, Pb_5^{2-}, Pb_9^{4-}, Sb_7^{3-}, Bi_4^{2-}, etc).[1-3] When countered with positively charged alkali or alkaline-earth atoms, the Zintl ions form salts. However, unlike traditional intermetallics and semiconductors, the Zintl phase is characterized by significant bonding between the Zintl ions. Due to their unexpected stoichiometry and fascinating structures, Zintl ions have been studied since 1930s.[4,5] Recent upsurge of research activity in Zintl ions is not only due to the observation that they can be extracted from the lattice and, when dissolved in appropriate solvents, can be used as reactants in solution chemistry, but also because they appear to be promising candidates for thermoelectric applications. For example, the cationic sites of the Zintl phase can be doped without strongly affecting the anionic network, thus allowing tailoring of the band gap.[6] Similarly, the large and complex structures of the anion moieties lead to low thermal conductivity, enhancing the figure of merit of thermoelectric materials.[6,7]

The composition and stability of traditional Zintl ions have been rationalized by the electron counting rules originally proposed by Wade[8,9] and later developed by Mingos[10,11] for understanding the structure and bonding of polyhedral borane clusters (B_nH_m). These species are considered to be electron deficient since they lack sufficient number of electrons for conventional covalent bonding between pairs of adjacent atoms. Thus, the concept of multi-center bonds was developed where valence electrons are separated into external and skeletal electrons.[1] The external electrons are assumed to form covalent bonds with external ligands in polyhedral boranes or nonbonding electron pairs in post transition element clusters. The skeletal electrons, on the other hand, are responsible for cage bonding. According to the Wade-Mingos rules, $2n+2$, $2n+4$, and $2n+6$ electrons are needed to form *closo*, *nido*, and *arachno* boranes where n is the number of vertices in the polyhedron, respectively. For example, in well-known icosahedral $B_{12}H_{12}^{2-}$ cluster, two electrons from each of the BH pair form covalent bonds while the other two electrons are contributed to cage bonding. Thus, with n = 12, there are 24 electrons that are available for cage bonding, but $2n+2$ electron rule requires a total of $2\times12+2 = 26$ electrons for stabilizing the *closo*-structure. Hence, $B_{12}H_{12}$ requires two extra electrons to be stable and $B_{12}H_{12}^{2-}$ exists as a di-anion.[1] In group 14 and 15 elements, one assumes that the two *s* electrons belong to the core and the *p* electrons form the valence shell.[12] Thus, in Sn_5^{2-} cluster there are $2\times5+2 = 12$ electrons and Sn_5^{2-} has a *closo*-structure with a polyhedron having 5 vertices.[3] In Bi_4^{2-} there are $4\times3+2 = 14$ electrons and the cluster has the *arachno*-structure ($2\times4+6 = 14$) with four vertices in the tetrahedron. Analogous to $B_{12}H_{12}^{2-}$ cluster Sn_{12}^{2-} also forms a *closo*-structure since Sn is isoelectronic with a BH pair and Sn_{12}^{2-} is an example of a cage Zintl ion.[13]

That the formation of Zintl ions in the gas phase could be inferred from photoionization mass spectral studies[15] has led to a paradigm shift in the search for new Zintl ions. Farley and Castleman[15] observed $(Na_4Bi_3)^+$ as a magic number in the mass

spectra of $Na_nBi_m^+$ clusters and attributed its unusual stability to be due to the presence of Bi_3^{3-} as a Zintl ion. A combination of photoelectron spectroscopy experiment and theoretical calculations has later identified the presence of Zintl ions Sn_4^{4-}, Ga_4^{2-}, Sn_{12}^{2-}, and Pb_{12}^{2-} in cluster anions of $(Na_3Sn_4)^-$, $(NaGa_4)^-$, $(KSn_{12})^-$, and $(KPb_{12})^-$, respectively.[16-19] The jellium electron counting rule[20] originally developed to explain the magic numbers in alkali metal clusters[21] has also been found to account for the stability of some Zintl ions.[22,23] In the jellium model, electrons fill a spherical potential well produced by a uniform distribution of positive ion cores and successive filling of $1S^2$ $1P^6$ $1D^{10}$ $2S^2$ $1F^{14}$ $2P^6$… shells give rise to shell closings at 2, 8, 20, 34, 40, … electrons. Bare clusters such as In_{11}^{7-} and Si_4^{4-} (or Pb_4^{4-}) can be represented as Zintl ions where jellium electron counting rule prevails since they contain 40 and 20 electrons, respectively.[22-24] Note that in the jellium model all the valence electrons are involved in skeletal bond formation. Recently, using photoelectron spectroscopy experiment and density functional theory calculations, Wang *et al*. showed that aluminum moieties within selected $Na_mAl_n^-$ clusters can also be classified as Zintl ions.[25] This observation demonstrates that electron counting rules other than that due to Wade and Mingos can also be used to design and synthesize a new class of Zintl ions.

While much of the earlier work on Zintl ions has concentrated on traditional group 13, 14, and 15 elements, during last decade a few endohedral clusters with transition metal (TM) atoms embedded inside post transition metal (PTM) cage skeletons have been experimentally synthesized (e.g. $Nb@As_8^{3-}$, $Pd_2@Sn_{18}^{4-}$, $Ni@Pb_{12}^{2-}$, $Pt@Pb_{12}^{2-}$, and $Ir@Sn_{12}^{3-}$).[14,26-29] These findings further extend the elemental constitution of Zintl anions beyond pure PTM atoms to a combination of PTM atoms and TM atoms. While some these $TM_m@PTM_n^{p-}$ ($p > 1$) Zintl anions obey the Wade-Mingos rules, a few of them do not obey any electron counting rule.

In this paper we raise a new question: can a Zintl-like ion composed of *only* transition metal atoms exist? If so, we may further enlarge the family of Zintl ions that could even be magnetic. Up to now, *all* TM atom-based Zintl ions are rare. This is because due to their low ionic potential energies, it is unusual for TM atoms to exhibit stable multiply negatively charged states. We note that the stability of compounds consisting of TM atoms is governed by the 18-electron rule which requires the filling of s^2, p^6, and d^{10} orbitals. Classic examples of compounds that obey the 18-electron rule are $Cr(C_6H_6)_2$, $Fe(C_5H_5)_2$, and $Au_{12}W$.[30,31] In the present study, we show that *all* TM based moieties capable of attracting multiple electrons can be designed using the 18-electron rule and such negative ions can be identified with the Zintl-like ions. We confirm their charge state by counter balancing them with appropriate number of alkali or alkaline earth metal atoms. Using first-principles calculations we first show that experimentally synthesized Mg_2FeH_6 crystal[32,33] is characteristic of a Zintl phase material and the existence of FeH_6^{4-} anion is consistent with the 18-electron rule. By replacing the H atoms with their isovalent Au atoms, forming a Mg_2FeAu_6 crystal, we find that the large electron transfer from Mg to $FeAu_6$ moiety still persists. This suggests the possibility that Zintl-like ions composed of all TM metal atoms can be designed. We show this indeed is the case. By choosing Na atoms as counter cations we show that $Na_2[Ti@Au_{12}]$ and $Na_2[Ni@Au_6]$ moieties are stable. In addition, $Ti@Au_{12}$ and $Ni@Au_6$ carry doubly negative charge, exhibiting characteristics of Zintl ions. We further show that when $Na_2[Ti@Au_{12}]$ and $Mg[Ti@Au_{12}]$ are respectively assembled into two-dimensional (2D) and one-dimensional (1D) periodic systems, their large charge transfer characters still remain. While the former is a semiconductor and non-magnetic, the latter is a metal and magnetic. Hence, the 2D $Na_2[Ti@Au_{12}]$ and 1D $Mg[Ti@Au_{12}]$ constitute a novel TM-based Zintl-like phase. This observation opens the door to the synthesis of a new class of TM-based Zintl-like phases with unique properties. In the following we describe our theoretical methods and results.

Computational Details

We have used a multi-scale approach to study the TM-based Zintl-like ions. For the study of the Zintl-like phase in crystalline solid as well as in the gas phase we have used first-principles calculations based on spin polarized density functional theory (DFT) implemented in Vienna *Ab initio* Simulation Package (VASP).[34] The exchange correlation energy is treated within the generalized gradient approximation (GGA) in the form proposed by Perdew, Burke, and Ernzerhof (PBE).[35] The projected augmented wave (PAW) method[36] with a cutoff energy of 300 eV is used. For periodic systems, we use Monkhorst-Pack special k point meshes with grid density of $2\pi\times0.02$ $Å^{-1}$ in their periodic directions to represent the reciprocal space.[37] For the low dimensional $Na_2[Ti@Au_{12}]$, $Mg[Ti@Au_{12}]$, and $Na_2[Ni@Au_6]$ systems, vacuum space of ~15 Å is applied along non-periodic directions. For the clusters, the reciprocal space is represented by the Γ point. The geometric structures are optimized by conjugated gradient method without any symmetry constraints. Convergence criteria of total energy and Hellmann-Feynman force on each atom are set to be 1×10^{-4} Å and 0.01 eV/Å, respectively. Bader's charge analysis method is used in order to achieve reliable electron population.[38]

To test the sensitivity of our results to theoretical methods and approximations, some of the results on clusters obtained from VASP calculations were re-computed using Gaussian 09 program[39] at the DFT/B3LYP level of theory. For Cs, Ti, and Au we used Stuttgart/Dresden ECPs (SDD) basis sets while for Na we used 6-31+G(D) basis. The geometries were optimized without symmetry constraints. The forces and total energies were converged to 3×10^{-4} eV/Å and 1×10^{-6} eV, respectively. The agreement between the results obtained from VASP and Gaussian 09 codes provides added confidence in the accuracy of our predictions.

Results and Discussion

The idea that the 18-electron rule can be used to design multiply negatively charged ions became apparent to us from recent work in complex hydrides which have been studied extensively for their potential to store large amounts of hydrogen.[33] In particular we focus on two examples, YMn_2H_6 and Mg_2FeH_6. The former has been synthesized from the Lave-phase metal hydride $YMn_2H_{4.5}$ with gaseous hydrogen under moderate conditions.[40]

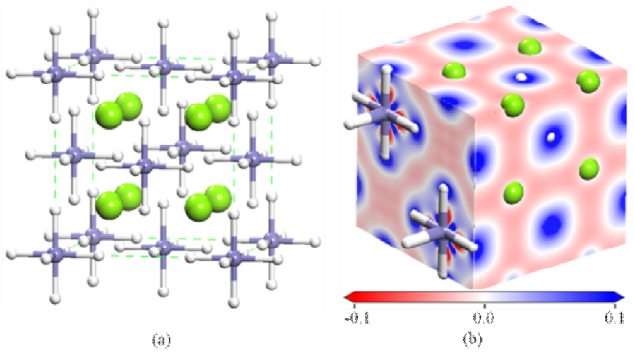

Fig. 1 (a) Crystal structure and (b) difference electron density distribution, $\Delta\rho$ (in 2D slice form, e/Å^3) of Mg_2FeH_6 crystal; green, cyan, and white spheres represent Mg, Fe, and H atoms, respectively. Green dashed lines indicate unit cell considered in our simulation.

One of the two Mn atoms in YMn_2H_6 in the unit cell forms an octahedral pentavalent $[MnH_6]^{5-}$ anion whose internal bonds are essentially covalent. Deficient five electrons are compensated by two cations, Y^{3+} and Mn^{2+}. In Mg_2FeH_6 crystal, if one assumes that the bonding between Fe and H is covalent and that between Mg and FeH_6 moiety is ionic, one would expect the charge on the FeH_6 moiety to be -4. Note that since Fe and Mn have, respectively, $3d^6\ 4s^2$ and $3d^5\ 4s^2$ configuration, the total number of electrons in both $[FeH_6]^{4-}$ and $[MnH_6]^{5-}$ are 18 and both the anions can be identified as Zintl-like anions. To confirm the charge state of FeH_6, our first objective was to study the electronic structure of Mg_2FeH_6 crystal. We began with the lattice constant and initial ionic positions known from experiment[32] and re-optimized the crystal structure using VASP code. After optimization, we find that the system retains its $Fm\bar{3}m$ symmetry space group (Figure 1a). The computed lattice parameter is 6.41 Å which agrees well with the previous theoretical result of 6.39 Å[32] and the experimental value of 6.44 Å, The cohesive energy E_{coh} is calculated using the equation $2E_{Mg^{2+}} + E_{FeH_6{}^{4-}} - E_{Mg_2FeH_6}$) is 21.17 eV per formula unit. In Figure 1b, we plot the difference electron density $\Delta\rho$ (= $\rho_{Mg2FeH6} - \rho_{Mg2} - \rho_{FeH6}$) to visualize its electron distribution; positive and negative values represent electron accumulation and depletion, respectively. It can be clearly seen that the valence electrons of Mg atoms are transferred to the FeH_6 moiety. This makes the Mg_2FeH_6 an ionically bonded crystal. Our band structure calculation also confirms that the Mg_2FeH_6 is a semiconductor with band gap of 1.9 eV (Figure S1 in ESI), consistent with previous calculations. In order to evaluate the charge state of each atom, we apply Bader's charge analysis. We find that on average each Mg atom loses 1.66 electrons, and each H (Fe) atom receives 0.52 (0.21) electrons, making the electronic configuration of the system $[Mg_2]^{+3.32}[FeH_6]^{-3.32}$. This result is consistent with what can be derived from the 18-electron rule and confirms that the $FeH_6{}^{4-}$ is a stable TM-based Zintl-like ion.

Since H and Au are isovalent and previous works have demonstrated that Au can mimic the properties of H in compounds,[41] we explored whether $[FeAu_6]^{4-}$ could behave like a Zintl-like ion and if so can a crystal of $Mg_2(FeAu_6)$ be stabilized with $Fm\bar{3}m$ symmetry. We optimized the crystal structure of $Mg_2(FeAu_6)$ and found that it retains its $Fm\bar{3}m$ symmetry (Figure S2). Bader's charge analysis shows that the two Mg atoms transfer 3.08 electrons to the $FeAu_6$ moiety, making the system $[Mg_2]^{+3.08}[FeAu_6]^{-3.08}$. This indicates that all TM-based moiety can possess Zintl-like character, consistent with the expectation of the 18-electron rule.

To see if the 18-electron rule can be generalized to yield Zintl-like ions composed of only transition metal atoms, we considered two endohedral clusters containing Au polyhedra. The first example we consider is $Ti@Au_{12}$, where Ti is embedded inside an Au_{12} cage. In this cluster, each Au contributes one electron and Ti, with electronic configuration $3d^24s^2$, contributes four valence electrons. Hence, in total there are 16 valence electrons and it needs two additional electrons to complete the 18-electron rule requirement. To find the ground state geometry of $[Ti@Au_{12}]^{2-}$ we began with four isomers with symmetry point group I_h, O_h, D_{5h}, and D_{3h} as starting points and optimized their structures without imposing symmetry constraints. The resulting optimized geometries are given in Figure 2. The I_h isomer is found to be stable among all other isomers and the isomer with O_h symmetry lies 0.136 eV higher in energy. To confirm that the stability of the I_h isomer is independent of our numerical procedure we took two close isomers obtained from VASP result and re-optimized the structures using Gaussian 09 program. We found that I_h isomer is 0.12 eV more stable than the O_h isomer, which is consistent with our VASP result. Since this energy difference is within the accuracy of the DFT/B3LYP level of theory, we calculated their IR and Raman spectra using the Gaussian 09 program so that they can be compared with future experiments to determine the true ground state configuration. The results are given in Figure S3 (ESI). Note that there is a marked difference between these spectra.

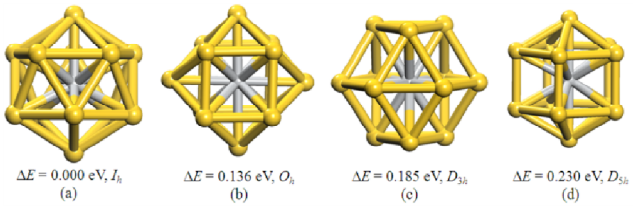

Fig. 2 Optimized geometries of four possible $[Ti@Au_{12}]^{2-}$ isomers with relative energies.

To confirm that $Ti@Au_{12}$ cluster would prefer to exist as a di-anion, we computed the equilibrium structure, energetics, and electron charge density distribution of $Na_2[Ti@Au_{12}]$. Note that due to their electropositive character alkali atoms are known to donate their electron. We began with a structure of $Na_2[Ti@Au_{12}]$ by adding two Na atoms on the surface of $Ti@Au_{12}$ neutral cluster. We considered four possible structures of $Ti@Au_{12}$ (with symmetry point group of I_h, O_h, D_{5h}, and D_{3h}) described in the above as cores and attached two Na atoms on different sites. In this way, we generated more than 30 different isomers. After structural optimization, no imaginary frequencies were found for these relaxed isomers. The three energetically lowest structures are shown in Figure 3. From these isomers, we see that the Na atoms tend to reside on the hollow site of square Au facets. In the lowest energy isomer, the core $Ti@Au_{12}$ exhibit a symmetry point group of O_h, and two Na atoms reside on two opposite square facets. The average Na-Au bond length in the relaxed configuration is 2.97 Å, and Au-Au bond lengths range between 2.77 and 2.85 Å. The symmetry point group of this $Na_2[Ti@Au_{12}]$ cluster is D_{4h}. The second (third) lowest energy isomer, which are

0.059 eV (0.061 eV) higher in energy than the ground state, is made up of D_{5h} (O_h) core Ti@Au_{12} unit, with two Na atoms also residing on two square facets. In order to explore the thermal stability of the Ti@Au_{12} and Na_2[Ti@Au_{12}], we performed *ab initio* molecular dynamic (AIMD) simulations with Nosé-Hoover heat bath at 300 K. The time step is set to be 1 fs and the AIMD lasts for 3000 steps. Following this simulation we found both Ti@Au_{12} and the Na_2[Ti@Au_{12}] systems to distort slightly, which can be optimized back to their static structures. The total energy fluctuations with respect to time are shown in Figure S4 (ESI). This shows that both the structures are thermodynamically stable at room temperature. We also used higher force convergence criterion of 0.0003 eV/Å and energy cutoff of 400 eV and re-optimize the three lowest isomers in Figure 3. We find that the structures remain almost unchanged, and the energy of structure in Figure 3b (Figure 3c) is higher than that of Na_2[Ti@Au_{12}]-D_{4h} (Figure 3a) by 0.058 (0.061) eV. This confirms the accuracy of our computation procedure. Here also we took D_{4h} isomer of Na_2[Ti@Au_{12}] which has been found to be lowest energy isomer

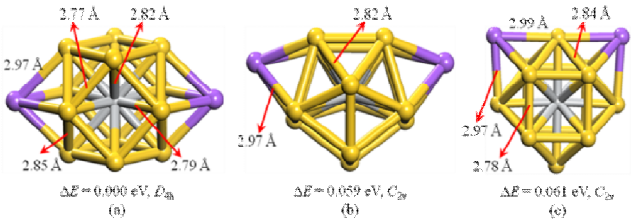

Fig. 3 The three lowest energy isomers of Na_2[Ti@Au_{12}] along with their relative energies, ΔE and symmetry point groups. The yellow, magenta, and light grey spheres represent Au, Na, and Ti, respectively. Some typical bond lengths are indicated by red arrows.

in VSAP optimization and re-optimized again using Gaussian 09. We found that the geometrical parameters are close to VASP results. For example Na-Au distance in Gaussian 09 calculation is 2.97 Å which is exactly same as that in VASP calculation. There are slight differences in other bond distances, but they lie within a range of 0.05 Å. So, for further discussion we only present results obtained from the VASP code.

In Figure 4 we plot the difference electron density $\Delta\rho$ (= $\rho_{Na2[Ti@Au12]} - \rho_{Na2} - \rho_{Ti@Au12}$), which shows a large amount electron transfer from Na to the Ti@Au_{12} moiety. This is expected because the electron affinity of Na (0.548 eV) is much smaller than that of Au (2.309 eV).[42] Using Bader's charge analysis, we find that each Na atom donates 0.83 electrons. As for the eight Au atoms bonded to Na, each of them receives ~0.29 electrons, and the other four Au atoms each receive ~0.19 electrons. The reason that the eight Na-bonded Au atoms carry more electrons is because of attractive electrostatic interaction between the negatively charged Au and the positively charged Na atom. The interstitial Ti atom is also positively charged and loses ~1.44 electrons. Hence, in total the Ti@Au_{12} moiety receives 1.66 electrons, making the electronic configuration of the system becomes $[Na_2]^{+1.66}[Ti@Au_{12}]^{-1.66}$. With this value, we demonstrate that the Ti@Au_{12} moiety is a Zintl-like ion, consistent with the 18-electron rule. We note that for the other energetically lower isomers, the amount of charge transfer from the Na to the Ti@Au_{12} moiety is also similar, which shows that its Zintl-like ion character is robust with respective to its geometric structure.

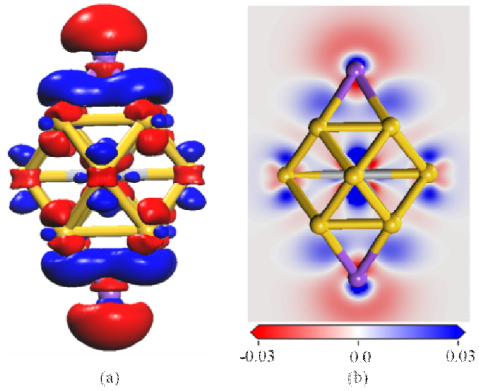

Fig. 4 (a) Isosurface (with value of 0.01 e/Å^3) and (b) 2D slice of electron difference density of Na_2[Ti@Au_{12}]. Blue and red colors indicate positive (electron accumulation) and negative (electron deficiency) values, respectively.

To further confirm that the preferred charge on Ti@Au_{12} is -2, we studied the relative stability of Na_n[Ti@Au_{12}] clusters (n = 1, 2, 3) by calculating the energy gain of adding successive Na atoms, namely,

$\Delta E_n = E[Na_{n-1}Ti@Au_{12}] + E[Na] - E[Na_nTi@Au_{12}]$, n = 1, 2, 3.

Here $E[Na_nTi@Au_{12}]$ is the energy of the Na_n[Ti@Au_{12}] cluster and E[Na] is the energy of the Na atom. The preferred charge state of Ti@Au_{12} can be obtained by determining which of the Na_n[Ti@Au_{12}] clusters is the most stable and for that stoichiometry what is the charge on the Ti@Au_{12} moiety. The computed values of ΔE_n are 2.56 eV, 2.57 eV, and 1.42 eV for n = 1, 2, and 3, respectively. The abrupt drop in the binding energy of the third Na atom in Na_n[Ti@Au_{12}] clearly shows that the Ti@Au_{12} moiety prefers to bind to two Na atoms. In other words, the preferred charge state of Ti@Au_{12} is -2 (dianion), rather than -3 (trianion). Same conclusion can be reached by comparing the energies needed to dissociate the Na_2[Ti@Au_{12}] into $2Na^+$ + Ti@Au_{12}^{2-} or Na^+ + NaTi@Au_{12}^-. These energies are respectively 12.65 eV and 4.99 eV. The substantial stability of Na_2[Ti@Au_{12}] where Ti@Au_{12}^{2-} exists as a di-anion provides further proof that the latter is a Zintl-like ion.

In order to further explore the electronic property of the Na_2[Ti@Au_{12}], we calculated its molecular orbital (MO) energy levels as shown in Figure 5. The energy gap between the highest occupied molecular orbital (HOMO) and the lowest unoccupied molecular orbital (LUMO) is 1.21 eV at the GGA-PBE level of theory. By plotting the wave functions of HOMO and LUMO orbitals we find that the HOMO is singly degenerated and contributed by Ti and all Au atoms, while the LUMO is triply degenerated and arises from Ti, Na as well as Na-bonded Au atoms. This can be furthermore verified by the projected density of states (PDOS, see Figure S5). We clearly observe that the HOMO is hybridized mainly by the Au-*s*, Au-*d*, and the Ti-d_{xy} orbitals, and the LUMO is contributed by hybridization among Au-*d*, Au-*p*, Na-*s*, and Ti-d_{z2} orbitals.

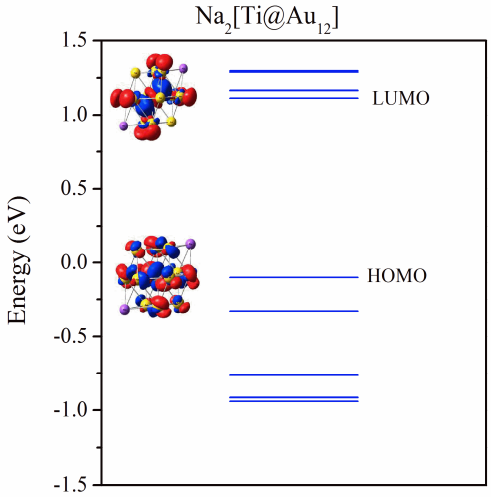

Fig. 5 Molecular orbital energy levels and HOMO and LUMO wave functions of $Na_2[Ti@Au_{12}]$.

To study the effect of cation moieties on the Zintl-like characteristics of $Ti@Au_{12}^{2-}$ we consider two other compensating cations, namely, Cs and Mg. For $Cs_2[Ti@Au_{12}]$ we find that the lowest energy structure is similar to that of $Na_2[Ti@Au_{12}]$ where the two Cs atoms reside on two opposite square facets of the O_h $Ti@Au_{12}$ cage (Figure S6). The symmetry point group of the $Cs_2[Ti@Au_{12}]$ is again D_{4h}. Based on Bader's charge analysis, each Cs atom donates ~0.82 electrons, and hence the $Ti@Au_{12}$ cage receives 1.64 electrons, forming $[Cs_2]^{+1.64}[Ti@Au_{12}]^{-1.64}$. Frontier molecular orbitals (HOMO and LUMO) of the $Cs_2[Ti@Au_{12}]$ are similar as that in $Na_2[Ti@Au_{12}]$ (Figure S8). For $Mg[Ti@Au_{12}]$, we find that Mg also prefers to reside on square facet of $Ti@Au_{12}$ (Figure S7). The Mg atom transfers 1.40 electrons to the $Ti@Au_{12}$ moiety, making the system $Mg^{+1.40}[Ti@Au_{12}]^{-1.40}$. These results demonstrate that the $Ti@Au_{12}$ is, indeed, a Zintl-like ion, satisfying the 18-electron rule.

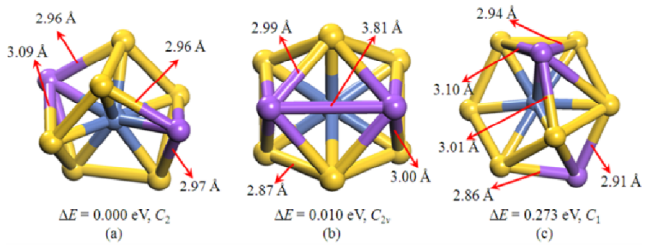

Fig. 6 The three lowest energy isomers of $Na_2[Ni@Au_6]$ along with their relative energies ΔE and symmetry point group. The yellow, magenta, and dark blue spheres represent Au, Na, and Ni, respectively.

To substantiate our hypothesis that the 18-electron rule can be used in general to design all TM-based Zintl-like ions, we consider another example, namely, $Ni@Au_6$. Since the Ni ($3d^84s^2$) contains 10 valence electrons, the total number of valence electrons of $Ni@Au_6$ cluster is 16, which again needs another two electrons to satisfy the 18-electron rule. Hence, we examine the geometric and electronic structure of $Na_2[Ni@Au_6]$. Various initial geometric structures are considered, and the lowest three energetic isomers are shown in Figure 6. We find that the ground state occurs when the two Na atoms reside on opposite sides of a distorted wheel-like $Ni@Au_6$ cluster, and the Na-Au bond lengths range between 2.96 Å and 3.09 Å. The symmetry point group is C_2. Bader's charge analysis reveals that each Na donates 0.83 electrons, so that the electronic configuration of this ground state structure becomes $[Na_2]^{+1.66}[Ni@Au_6]^{-1.66}$. The second lowest energy structure is higher than the ground state by 0.01 eV, where the two Na atoms reside on the same side of the $Ni@Au_6$ polyhedron and the symmetry point group is C_{2v}. This energy difference corresponds to a temperature of 116 K, indicating that this isomer can also been found experimentally. In this structure, each Na atom transfers ~0.84 electrons to the $Ni@Au_6$ moiety, and the electronic configuration of this isomer is $[Na_2]^{+1.68}[Ni@Au_6]^{-1.68}$. Hence the $Ni@Au_6$ moiety is a Zintl-like ion, satisfying the 18-electron rule.

In order to examine if the previous conclusion still holds in periodic systems, we designed a two-dimensional (2D) $Na_2[Ti@Au_{12}]$ structure. Figure 7a shows the relaxed geometry, which is found to belong to *P4/mm* plane symmetry group. The bond length between the Na and the Au is 2.92 Å, a little shorter than that in the cluster form. The cohesive energy E_{coh} ($=2E_{Na^+} + E_{Ti@Au_{12}^{2-}} - E_{Na_2[Ti@Au_{12}]}$) is calculated to be 3.58 eV per simulated unit cell. Bader's analysis shows each Na transfers 0.77 electrons to the $Ti@Au_{12}$ moiety, confirming its Zintl-like character. Band structure calculation (Figure 7b) indicates that the 2D $Na_2[Ti@Au_{12}]$ is an indirect-gap semiconductor with band gap of 0.55 eV. The valence band maximum (VBM) and conductance band minimum (CBM) are located at the M and Γ point, respectively.

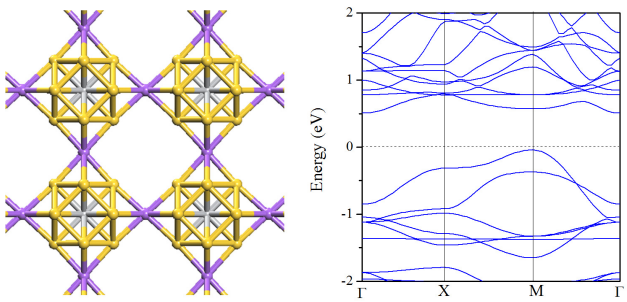

Fig. 7 (a) Geometry and (b) band structure dispersion of 2D $Na_2[Ti@Au_{12}]$ along high symmetry points Γ (0, 0, 0) to X (1/2, 0, 0), M (1/2, 1/2, 0), and to Γ.

For a periodic $Mg[Ti@Au_{12}]$ Zintl-like phase, we consider a 1D periodic chain. The relaxed structure is shown in Figure 8a. We see that the Au atoms in different $Ti@Au_{12}$ moieties are bonded together. The cohesive energy E_{coh} ($= E_{Mg^{2+}} + E_{Ti@Au_{12}^{2-}} - E_{Mg[Ti@Au_{12}]}$) is calculated to be 12.82 eV per simulated unit cell. This value is larger than that of 2D-$Na_2[Ti@Au_{12}]$ because of bond formation between Au atoms in different $Ti@Au_{12}$ moieties. Charge analysis shows that each Mg donates 1.79 electrons to each $Ti@Au_{12}$. We find that the Ti atoms are magnetic carrying a moment of 0.66 μ_B, contributed primarily by their d_{z2} orbitals (Figure 8b). Ferromagnetic coupling between the Ti atoms is calculated to be more stable than antiferromagnetic coupling by 0.025 eV per unit cell, which corresponds to a temperature of 290 K. We attribute the ferromagnetic coupling to hybridization

between the Au-*s* and Ti-*d* orbitals. Band dispersions of both spin up and spin down channels are also plotted (Figure 8c) showing that the 1D Mg[Ti@Au_{12}] chain is metallic in both spin channels. In contrast, conventional Zintl phase materials are semiconducting and paramagnetic. The origin of the magnetic and metallic properties of 1D Mg[Ti@Au_{12}] is due to the fact that the anionic moieties, Ti@Au_{12}, are bonded together, instead of separated by alkali or alkaline-earth metal atoms as is the case in conventional Zintl phases.

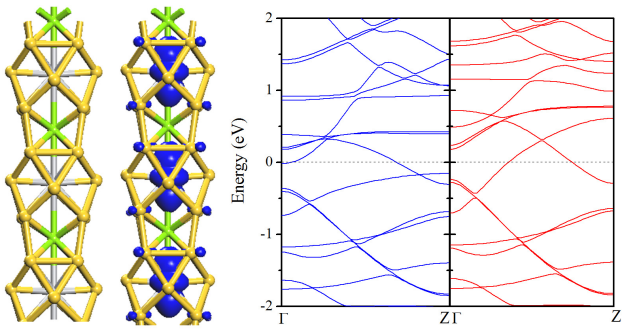

Fig. 8 (a) Geometry, (b) spin density (isosurface value of 0.01 e/Å^3), and (c) band structure of 1D Mg[Ti@Au_{12}]. Blue and red curves in the band structure plot represent spin up and spin down channel, respectively.

Conclusions

In summary, we show for the first time that Zintl-like ions composed of *only* TM atoms can be realized by using the 18-electron rule. This is demonstrated by first performing the Bader's charge analysis in complex metal hydride, Mg_2FeH_6 and demonstrating that FeH_6 prefers a charge state of -4. Since H and Au are isoelectronic, it is expected that Mg_2FeAu_6 may have similar properties as that of Mg_2FeH_6. Calculations indeed confirmed this to the case. We note that $[FeAu_6]^{4-}$ is an all transition metal moiety that is Zintl-like and consistent with the 18-electron rule. To generalize the concept that Zintl-like ions composed of all TM atoms are possible, we carried out first-principle calculations based on gradient corrected density functional theory by focusing on Na_2[Ti@Au_{12}], Mg[Ti@Au_{12}], Cs_2[Ti@Au_{12}], and Na_2[Ni@Au_6] clusters. These clusters are shown to be very stable with ionic bonding between the cationic (Na^+, Cs^+, Mg^{2+}) and anionic components (Ti@Au_{12}^{2-}, Ni@Au_6^{2-}). Bader's charge analysis further shows that these anionic components are di-anions, making Ti@Au_{12}^{2-} and Ni@Au_6^{2-} candidates for forming the Zintl-like phase. This is demonstrated by constructing 2D and 1D periodic structures of Na_2[Ti@Au_{12}] and Mg[Ti@Au_{12}], respectively. The former is found to be a nonmagnetic semiconductor, while the latter is a ferromagnetic metal. That the 18-electron rule can be used to design Zintl-like ions composed of *all* TM atoms furthers the scope of the Zintl ions and opens the door to the synthesis of new Zintl phase compounds. Periodic structures formed from these Zintl-like transition metal moieties exhibit unique electronic and magnetic properties. The ability to tailor the cationic and anionic components of the Zintl salts may have potential applications in solution chemistry as well as in thermoelectric materials.

Acknowledgments

Research was supported by the U.S. Department of Energy, Office of Basic Energy Sciences, Division of Materials Sciences and Engineering under Award # DE-FG02-96ER45579. We also acknowledge resources of the National Energy Research Scientific Computing Center, which is supported by the Office of Science of the U.S. Department of Energy under Contract No. DE-AC02-05CH11231.

Notes and references

[a] *Physics Department, Virginia Commonwealth University, Richmond, VA 23284 USA. E-mail: pjena@vcu.edu*

† Electronic Supplementary Information (ESI) available: Band structure of Mg_2FeH_6, structure of Mg_2FeAu_6, IR and Raman spectra of [Ti@Au_{12}]$^{2-}$, PDOS of Na_2[Ti@Au_{12}], molecular orbitals of Cs_2[Ti@Au_{12}] and isomers of Cs_2[Ti@Au_{12}] and Mg[Ti@Au_{12}]. See DOI: 10.1039/b000000x/

1 T. F. Fässler, *Zintl Phases: Principles and Recent Developments*; Springer: Heidelberg, 2011.
2 S. Scharfe, F. Kraus, S. Stegmaier, A. Schier and T. F. Fässler, *Angew. Chem. Int. Ed.* 2011, **50**, 3630 - 3670.
3 J. D. Corbett, *Chem. Rev.* 1985, **85**, 383 - 397.
4 E. Zintl, J. Goubeau and W. Dullenkopf, *Z. Phys. Chem. Abt. A* 1931, **154**, 1 - 46.
5 E. Zintl and H. Kaiser, *Z. Anorg. Allgem. Chem.* 1933, **211**, 113 - 131.
6 L. Zhang, M.-H. Du and D. J. Singh, *Phys. Rev. B* 2010, **81**, 075117 - 075124.
7 S. M. Kauzlarich, S. R. Brown and G. J. Snyder, *Dalton Trans.* 2007, 2099 - 2107.
8 K. Wade, *J. Chem. Soc. D: Chem. Commun.* 1971, 792 - 793.
9 K. Wade, *Adv. Inorg. Chem. Radiochem.* 1976, **18**, 1 - 66.
10 D. M. P. Mingos, *Acc. Chem. Res.* 1984, **17**, 311 - 319.
11 D. M. P. Mingos and R. L. Johnston, *Struct. Bond.* 1987, **68**, 29 - 87.
12 R. G. Wheeler, K. LaiHing, W. L. Wilson and M. A. Duncan, *J. Chem. Phys.* 1988, **88**, 2831 - 2839.
13 N. Shao, S. Bulusu and X. C. Zeng, *J. Chem. Phys.* 2008, **128**, 154326 - 154333.
14 Z.-M. Sun, H. Xiao, J. Li and L.-S. Wang, *J. Am. Chem. Soc.* 2007, **129**, 9560 - 9561.
15 R. W. Farley and A. W. Castleman Jr., *J. Am. Chem. Soc.* 1989, **111** , 2734 - 2735.
16 W. J. Zheng, O. C. Thomas, J. M. Nilles, K. H. Bowen, A. C. Reber and S. N. Khanna, *J. Chem. Phys.* 2011, **134**, 224307 - 224315.
17 A. E. Kuznetsov, A. I. Boldyrev, X. Li and L. S. Wang, *J. Am. Chem. Soc.* 2001, **123**, 8825 - 8831.
18 L. F. Cui, X. Huang, L. M. Wang, D. Y. Zubarev, A. I. Boldyrev, J. Li and L. S. Wang, *J. Am. Chem. Soc.* 2006, **128**, 8390 - 8391.
19 L. F. Cui, X. Huang, L. M. Wang, J. Li and L. S. Wang, *J. Phys. Chem. A* 2006, **110**, 10169 - 10172.
20 M. Brack, *Rev. Mod. Phys.* 1993, **65**, 677 - 732.
21 W. D. Knight, K. Clemenger, W. A. de Heer, W. A. Saunders, M. Y. Chou and M. Cohen, *Phys. Rev. Lett.* 1984, **52**, 2141 - 2144.
22 S. C. Sevov and J. D. Corbett, *Inorg. Chem.* 1991, **30**, 4875 - 4877.
23 T. Goebel, Y. Prots and F. Haarmann, *Z. Kristallogr. New Cryst. Struct.* 2008, **223**, 187 - 188.
24 L. M. Molina, J. A. Alonso and M. J. Stott, Solid. State Commun. 1998, **108**, 519 – 524.
25 H. Wang, X. Zhang, Y. J. Ko, A. Grubisic, X. Li, G. Ganteför, H. Schnöckel, B. W. Eichhorn, M. S. Lee, P. Jena, A. K. Kandalam, B. Kiran and K. H. Bowen, *J. Chem. Phys.* 2014, **140**, 054301 - 054312.
26 H.-G. von Schnering, J. Wolf, D. Weber, R. Ramirez and T. Meyer, *Angew. Chem. Int. Ed.* 1986, **25**, 353 - 354.
27 E. N. Esenturk, J. Fettinger and B. Eichhorn, *J. Am. Chem. Soc.* 2006, **128**, 9178 - 9186.
28 E. N. Esenturk, J. Fettinger, Y.-F. Lam and B. Eichhorn, *Angew. Chem. Int. Ed.* 2004, **43**, 2132 - 2134.

29 J.-Q. Wang, S. Stegmaier, B. Wahl and T. F. Fässler, *Chem. Eur. J.* 2010, **16**, 1793 - 1798.
30 P. J. Pyykkö, *Organ. Chem.* 2006, **691**, 4336 - 4340.
31 X. Li, B. Kiran, J. Li, H.-J. Zhai and L.-S. Wang, *Angew. Chem. Int. Ed.* 2002, **41**, 4786 - 4789.
32 J.-J. Didisheim, P. Zolliker, K. Yvon, P. Fischer, J. Schefer, M. Gubelmann and A. F. Williams, *Inorg. Chem.* 1984, **23**, 1953 - 1957.
33 K. Miwa, S. Takagi, M. Matsuo and S. Orimo, *J. Phys. Chem. C* 2013, **117**, 8014 - 8019.
34 G. Kresse and J. Furthmüller, *Phys. Rev. B* 1996, **54**, 11169 - 11186.
35 J. P. Perdew, K. Burke and M. Ernzerhof, *Phys. Rev. Lett.* 1996, **77**, 3865 - 3869.
36 P. E. Blöchl, *Phys. Rev. B* 1994, **50**, 17953 - 17979.
37 H. J. Monkhorst and J. D. Pack, *Phys. Rev. B* 1976, **13**, 5188 - 5192.
38 W. Tang, E. Sanville and G. Henkelman, *J. Phys.: Condens. Matter* 2009, **21**, 084204 - 084210.
39 M. J. Frisch, G. W. Trucks, H. B. Schlegel, *et al.*, GAUSSIAN 09, Revision B.01, Gaussian, Inc., Wallingford, CT, 2010.
40 M. Matsuo, K. Miwa, S. Semboshi, H.-W. Li, M. Kano and S. Orimo, *Appl. Phys. Lett.* 2011, **98**, 221908 - 221910.
41 T. Zhao, Y. Li, Q. Wang and P. Jena, ChemPhysChem 2013, **14**, 3227 – 3232.
42 J. A. Dean, *Lange's Handbook of Chemistry*, 15th Ed.; McGraw-Hill: New York, 1999.